ACS OMEGA

Open Access

http://pubs.acs.org/journal/acsodf

Article

Methane–Water Interfacial Tension in Nanopores: A Dissipative Particle Dynamics Study

Fei Mo,* Zhilin Qi, Xiaoliang Huang, Wende Yan, Wanliang Zhang, Chaowen Wang, and Wenting Fu

Cite This: *ACS Omega* 2024, 9, 30794–30803

Read Online

ACCESS | Metrics & More | Article Recommendations

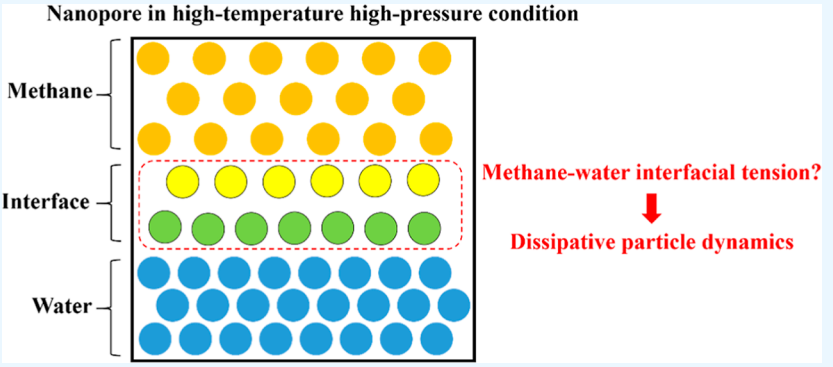

ABSTRACT: Imbibition of fracturing fluid in deep shale nanopores has a significant effect on shale gas production. One of the key parameters affecting imbibition is the interfacial tension of the methane–water system. However, studies on the methane–water interfacial tension in nanopores are very limited, and obtaining the accurate value of the methane–water interfacial tension at the nanoscale is difficult and time-consuming. In this work, a dissipative particle dynamics simulation model was built to study the methane–water interfacial tension in nanopores. This model provides reliable access to methane–water interfacial tension for deep shales under high-temperature, high-pressure conditions at low computation cost. It can be easily used to compute the methane–water interfacial tension in nanopores or the confined space in wide application scenarios. A sensitivity study of methane–water interfacial tension on a variety of factors was conducted. Results demonstrate that under high-pressure conditions, the increase in pressure leads to the rise of interfacial tension. When pressure increases from 20 to 120 MPa, interfacial tension rises from 0.0275 to 0.12 N/m, which contributes to the severe imbibition of fracturing fluid in deep shales. The confinement effect was observed by investigating the influence of pore size. Interfacial tension almost remains unchanged in pores smaller than 7 nm because most of the confined space is occupied by interface layer molecules in these pores. When pore size increases from 7 to 15 nm, the confinement effect is reduced. The interfacial tension experiences a growth from 0.1155 to 0.27 mN/m. Compared with pressure and pore size, the effect of temperature on interfacial tension can be neglected during deep shale gas production.

1. INTRODUCTION

Deep shale gas is referred to as the shale gas buried over 3500 m under the surface, which is in a high-temperature, high-pressure environment. In the Sichuan Basin, deep shale gas accounts for over 80% of the total shale gas resources,[1] which is a promising growth in gas energy production in China. Effective development of deep shale gas is of great importance. Due to the ultralow permeability, one of the main techniques to produce deep shale gas is hydraulic fracturing. However, after hydraulic fracturing, the majority of fracturing fluid is retained in the subsurface, with 15–40% recovery of injected water in deep shale gas reservoirs in China.[2] Some fracturing fluid is imbibed into the shale matrix due to the high capillary pressure inside the shale nanopores.[3−7] According to our previous studies,[8,9] water in shales significantly affects gas flow capability and gas production.

The imbibition of fracturing fluid is closely related to capillary pressure in the deep shale matrix. One of the key parameters affecting capillary pressure is the interfacial tension between methane and water in deep shales under high-temperature and high-pressure conditions. The methane–water interfacial tension in deep shales is difficult to be accurately obtained due to the following three reasons: (1) in the confined space (i.e., nanopores) of deep shale matrix, the value of interfacial tension

Received: April 8, 2024
Revised: June 20, 2024
Accepted: June 25, 2024
Published: July 3, 2024

is affected by pore size. Because interfacial tension is actually the sum of forces exerted on interface layer molecules by molecules outside the interface layers. In nanopores, the quantity of molecules outside the interface layers is limited due to the restriction of pore size. As a result, the study of interfacial tension in deep shales needs to consider the influence of pore size. (2) The high-temperature and high-pressure conditions make it extremely difficult to measure interfacial tension by experiments because it requires high-quality experimental apparatus, facilities, and strictly designed procedure. (3) In addition, the fluid state in deep shales could be different from conventional reservoirs due to the combined effects of confined space and high-temperature high-pressure environment. As a result, obtaining the reliable value of methane−water interfacial tension at the nanoscale under high-temperature and high-pressure conditions is a big challenge.

The interfacial tension under conventional conditions has been studied by many researchers through experiments and simulation. The most widely used experimental methods are the pendant drop method[10−12] and the Wilhelmy plate method.[13,14] However, the use of these two methods is restricted by pressure, fluid properties, the accuracy of the apparatus, etc. The pressure reported in the pendant drop method is up to 44.8 MPa,[15] which is still far below the pressure in deep shales. The Wilhelmy plate method can measure interfacial tension directly using a high-accuracy probe on the plate. In order to obtain reliable data, the density difference between two sorts of tested fluids should be less than 0.4 g/cm^3.[16] Besides, the accuracy and sensitivity of the probe also limit the application of this method. Therefore, the Wilhelmy plate method is usually utilized in liquid−liquid systems and is still not suitable for the methane−water system in deep shales. Other experiments such as the maximum bubble pressure method and the spinning drop method are also not applicable for deep shales. The maximum bubble pressure method is limited by the test pressure.[17] The spinning drop method can only be used to test ultralow interfacial tension, i.e., lower than 10^{-3} mN/m.[18] Therefore, obtaining the accurate interfacial tension of the methane−water system for deep shales through experimentation is difficult.

Molecular dynamics has usually been used to calculate interfacial tension in recent years. Dreher et al.[19] used molecular dynamics to study the interfacial tension of graphene−water system. They found that the value of interfacial tension is related to the area of the interface. Ghoufi and Malfreyt[20] investigated the interfacial tension at graphene−water interfaces. They reported that the simulated graphene−water interfacial tension is in line with the experimental water contact angle. Chiricotto et al.[21] reported that temperature affects the interfacial tension of a solid−liquid system via molecular dynamics simulation. The value of interfacial tension decreases with an increase of temperature. Li and Jin[22] studied hydrocarbon−water interfacial tension up to 500 MPa. They found that methane−water interfacial tension decreases with increasing pressure under low-pressure conditions. However, as the pressure further increases, the interfacial tension gradually rises. Doan et al.[23] also utilized molecular dynamics simulation to study the methane−water interfacial tension at a wide range of pressure (1 to 70 MPa). Their results indicate that the methane−water interfacial tension increases slightly when pressure exceeds 50 MPa at 323 K, which is consistent with the findings reported by Kvamme et al.[24] Guo et al.[25] investigated the interfacial tension of a methane−brine system with an ion mass fraction up to 25%. They found that the interfacial tension decreases with the rise of pressure (1 to 10 MPa) and is enlarged with the presence of ions. Naeiji et al.[26] conducted molecular dynamics simulations to study the interfacial behavior of a multicomponent gas mixture−water system. Although molecular dynamics can be used to compute the interfacial tension at the microscopic scale, its use requires a high-performance computer. Otherwise, computations can be very time-consuming.

In the petroleum industry, dissipative particle dynamics (DPD) simulation is used to study the interfacial tension of the fluid−fluid system. In DPD simulation, fluids with interfaces can be simulated using a set of particles (beads) that interact via conservative (nondissipative) force, dissipative force, and random force.[27] Deguillard et al.[28] applied DPD simulation to compute the interfacial tension in oil−water−surfactant systems. Rezaei and Modarress[29] utilized DPD simulation to study the hydrocarbon−water interfacial tension. Their results are in agreement with the experimental data. Wang et al.[30] investigated the effects of the ionic surfactant and the polymer on the oil−water interface using DPD simulation. Compared with the conventional molecular dynamics simulation, the DPD simulation is able to accurately calculate the interfacial tension of hydrocarbon−water systems with less computational cost.[29] Although DPD simulation has been used in a conventional fluid−fluid system, its application in confined space under high-temperature and high-pressure conditions has rarely been reported.

In this work, a DPD simulation model was established to study the interfacial tension of the methane−water system in deep shales at the nanoscale. This model provides convenient and reliable access to methane−water interfacial tension in nanopores under high-temperature and high-pressure conditions. The influences of temperature, pressure, and confined pore space on interfacial tension were investigated.

2. METHODS

DPD is originally a sort of coarse-grained meshless, particle-based, mesoscopic simulation which can be used to simulate a complex system using interacting particles (beads).[31] The beads interact with each other via conservative (nondissipative) force, dissipative force, and random force. The total force acting on a bead is expressed as[27]

$$\mathbf{f}_i = \mathbf{f}_i^{\mathrm{int}} + \mathbf{f}_i^{\mathrm{ext}} \tag{1}$$

where $\mathbf{f}_i$ is the total force acting on the ith bead; $\mathbf{f}_i^{\mathrm{int}}$ is the interparticle force acting on the ith bead; $\mathbf{f}_i^{\mathrm{ext}}$ is the external force acting on the ith force. The interparticle force $\mathbf{f}_i^{\mathrm{int}}$ consists of conservative (nondissipative) force $\mathbf{F}_{ij}^{\mathrm{C}}$, dissipative force $\mathbf{F}_{ij}^{\mathrm{D}}$, and random force $\mathbf{F}_{ij}^{\mathrm{R}}$

$$\mathbf{f}_i^{\mathrm{int}} = \mathbf{F}_{ij}^{\mathrm{C}} + \mathbf{F}_{ij}^{\mathrm{D}} + \mathbf{F}_{ij}^{\mathrm{R}} \tag{2}$$

where $\mathbf{F}_{ij}^{\mathrm{C}}$ is the conservative force exerted on the ith bead by the jth bead; $\mathbf{F}_{ij}^{\mathrm{D}}$ is the dissipative force exerted on the ith bead by the jth bead; $\mathbf{F}_{ij}^{\mathrm{R}}$ is the random force exerted on the ith bead by the jth bead.[29]

$$\mathbf{F}_{ij}^{\mathrm{C}} = a_{ij}\omega^{\mathrm{C}}(r_{ij})\hat{\mathbf{r}}_{ij} \tag{3}$$

where a_{ij} is the magnitude of the repulsive interaction strength between beads i and j. $\omega^{\mathrm{C}}(r_{ij})$ is the weight function for the conservative force; $\mathbf{r}_{ij}$ is the position vector; $r_{ij} = |\mathbf{r}_{ij}|$; $\hat{\mathbf{r}}_{ij}$ is the unit vector in the direction of $\mathbf{r}_{ij}$, which is expressed as

https://doi.org/10.1021/acsomega.4c03364
ACS Omega 2024, 9, 30794−30803

$$\hat{r}_{ij} = \frac{\mathbf{r}_{ij}}{|\mathbf{r}_{ij}|} \tag{4}$$

The dissipative force is written as[27]

$$\mathbf{F}_{ij}^{D} = -\gamma\omega^{D}(r_{ij})(\mathbf{v}_{ij}\cdot\hat{\mathbf{r}}_{ij})\hat{\mathbf{r}}_{ij} \tag{5}$$

where γ is the dissipation coefficient; $\omega^{D}(r_{ij})$ is the dissipation weight function. $\mathbf{v}_{ij}$ is the velocity vector. The random force $\mathbf{F}_{ij}^{R}$ is expressed as[29]

$$\mathbf{F}_{ij}^{R} = \sigma\omega^{R}(r_{ij})\xi_{ij}\Delta t^{-0.5}\hat{\mathbf{r}}_{ij} \tag{6}$$

where σ is the random force amplitude coefficient; $\omega^{R}(r_{ij})$ is the fluctuation weight function; ξ_{ij} is a random variable; Δt is the time step. There is a relation among $\omega^{C}(r_{ij})$, $\omega^{D}(r_{ij})$, and $\omega^{R}(r_{ij})$[32]

$$\omega^{C}(r_{ij}) = \omega^{R}(r_{ij}) = [\omega^{R}(r_{ij})]^{0.5} = \begin{cases} 1 - r_{ij}/r_{C}, & r_{ij} \le r_{C} \\ 0, & r_{ij} > r_{C} \end{cases} \tag{7}$$

where r_C is the effective interaction range or cutoff distance. The fluctuation−dissipation relationship requires[33]

$$\omega^{D}(r_{ij}) = [\omega^{R}(r_{ij})]^{2} \tag{8}$$

and

$$\gamma = \frac{\sigma^{2}}{2k_{B}T} \tag{9}$$

where k_B is the Boltzmann constant; T is the temperature. Based on Rezaei and Modarress's study,[29] the value of a_{ij} is essential to a successful DPD simulation, which is written as

$$a_{ij} = a_{ii} + b\chi_{ij} \tag{10}$$

where b is reported to be 3.5 and 1.45 if DPD number density is 3 and 5.[32,34] χ_{ij} is the Flory−Huggins parameter measured using thermally induced phase separation.[30] a_{ii} is expressed as

$$a_{ii} = [(\kappa^{-1}(T)N_{m} - 1)/2\alpha\rho]k_{B}T \tag{11}$$

where N_m is the coarse-graining degree, which is the number of molecules grouped in a DPD bead. α is a constant equal to 0.101; ρ is the DPD number density; κ^{-1} is the inversed dimensionless compressibility of the system

$$\kappa^{-1} = \frac{1}{k_{B}T}\left(\frac{\partial p}{\partial \rho}\right)_{T} \tag{12}$$

where p is pressure, which can be simplified as[35]

$$p = \frac{k_{B}T}{r_{C}^{3}}\overline{p} \tag{13}$$

$\overline{p}$ is dimensionless DPD pressure, which is expressed as

$$\overline{p} = \overline{\rho} + \alpha a\overline{\rho}^{2} \tag{14}$$

Based on the definition of interfacial tension, the interfacial tension perpendicular to the axis z is[29,36]

$$\lambda = \frac{L_z}{2}\left[\overline{p}_{zz}(t) - \frac{\overline{p}_{xx}(t) + \overline{p}_{yy}(t)}{2}\right] \tag{15}$$

where L_z stands for the length of the lattice along axis z. p_{xx}, p_{yy}, and p_{zz} are the stress tensors in the x, y, and z directions, which can be calculated using eq 14. Therefore, the interfacial tension of the methane−water interface tension can be obtained by simulating a lattice of methane and water beads with an interface perpendicular to axis z using a DPD study, and the value of the interfacial tension can be calculated using eq 15.

3. MODEL ESTABLISHMENT

In this section, a model for DPD simulation was established to calculate methane−water interfacial tension in nanopores of deep shales from the Longmaxi Formation in China. The simulation was conducted using the software *Materials Studio 8.0*.[37] The dimension of the simulation cell was 5 nm × 5 nm × 5 nm, which is in accordance with the majority pore size in the Longmaxi Formation.[38] We defined two types of beads to represent fluids. Bead W stands for the water molecule, and bead G represents the gas molecule. Basic information on each type of bead is exhibited in Table 1. Because one bead is not directly in contact with another, the surface properties of the beads are neglected in this model. The number of each type of bead is dependent on fluid densities and saturations. Under the real reservoir conditions (100 MPa, 423.15 K), the densities of methane and water are 0.276 and 0.965 g/cm^3, respectively. Water saturation is around 25%, and gas saturation is 75% in shales.[39] Therefore, we initially placed 975 Beads G and 1009 Beads W within one cell with an interface (Figure 1) to ensure the real densities and saturations of the fluids. We set this system under the reservoir conditions for DPD simulation to make it reach its minimal energy. After the interactions of beads, the energy of the system was the lowest. The state of the system

Table 1. Basic Information for the Bead Definition[a]

bead	mass (amu)	radius (Å)
G	16	2.07
W	18	1.38

[a]W for the water molecule and G for the methane molecule.

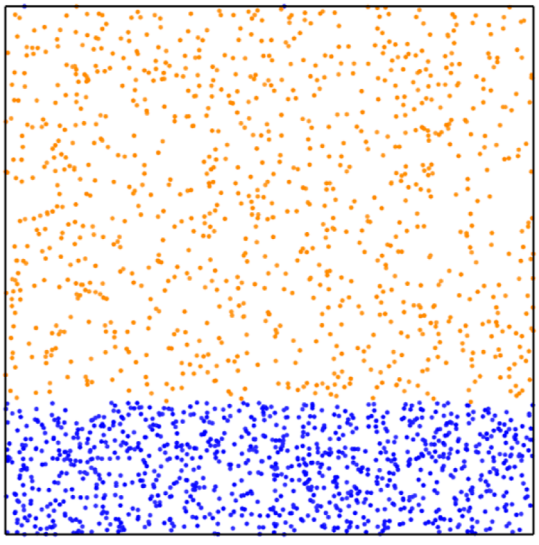

Figure 1. Initial state of the methane−water system at 100 MPa, 423.15 K. Orange bead (bead G) stands for the methane molecule. Blue bead (bead W) represents the water molecule.

https://doi.org/10.1021/acsomega.4c03364
ACS Omega 2024, 9, 30794−30803

reached equilibrium (Figure 2). The methane−water interfacial tension was finally calculated using the pressure tensors in eq 15.

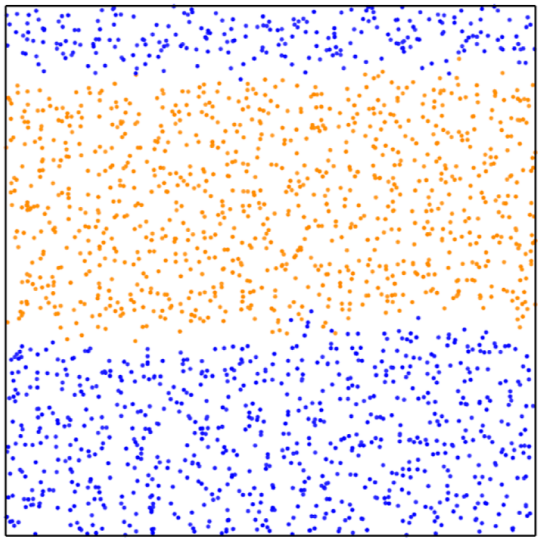

Figure 2. Equilibrium state of the methane−water system at 100 MPa, 423.15 K. Orange bead (bead G) stands for the methane molecule. Blue bead (bead W) represents water molecule.

DPD parameters for simulation are shown in Tables 2 and 3.[29,30] Based on the study of Wang et al.,[30] a_{ij} was set to 25 for all pair interactions between the same type of beads. The value of a_{ij} between Beads W and G was calculated using eq 10, in which χ_{ij} was determined through the DPD study on interfacial tension in the hydrocarbon−water system conducted by Rezaei and Modarress.[29] Rezaei and Modarress[29] calculated the values of χ_{ij} as a function of the number of water molecules in a bead. In our study, one bead contained a water molecule. Therefore, the value of χ_{ij} was set to 6.26 in Table 3.

Table 2. Repulsive Interaction Strength a_{ij} Used in the Simulation[a]

	G	W
G	25	40
W	40	25

[a]W for the water molecule and G for the methane molecule.

In order to calculate the stress tensors, the model was solved using the numerical integration method (the Velocity−Verlet method), which enables the calculation of the velocity, location, and forces of a particle at the next time step using the values at the present time step. The solution in this work was carried out using the software *Materials Studio 8.0*[37] through the following steps: (1) define the bead types for fluids. Bead W stands for the water molecule, and bead G represents the methane molecule. The parameters are shown in Table 1. (2) Build mesomolecules; the parameter (N_m) is exhibited in Table 3. (3) Build mesostructure; the parameters are exhibited in Table 3. After this step, a mesostructure packed with fluids was built. (4) Set the DPD force field; the parameters are shown in Table 2. (5) Solution; the parameters are displayed in Table 3. Through this process, the stress tensors in the *x*, *y*, and *z* directions were output by *MS*. After that, interfacial tension was computed using eq 15.

Table 3. Other DPD Parameters for the Simulation

parameter	value
N_m	1
r_c	1
χ_{ij}	6.26
length of simulation cell in the *x*, *y*,and *z* directions (nm)	5
reservoir temperature (K)	423.15
reservoir pressure (MPa)	100
methane density at reservoir temperature and pressure (kg/m^3)	276
water density at reservoir temperature and pressure (kg/m^3)	965
Δt (fs)	1
duration (ps)	200

4. MODEL VERIFICATION

The model was verified using Heuer's experimental data,[40] the nomograph proposed by Schowalter,[16] and the molecular dynamics simulation conducted by Li and Jin.[22]

Heuer[40] conducted experiments to measure interfacial tensions in a gas (95% methane, 5% ammonia)−water system at a series of pressures. In order to compare our model with Heuer's experimental results,[40] we calculated the interfacial tension under their experimental conditions (Table 4 and Figure 3) using our model. Fluid densities used in our simulation came from the NIST Chemistry WebBook (Table 4). Other parameters are shown in Tables 1−3. Compared with the experimental results, the error of our model ranges from 3.34 to 9.26% (Table 4).

Schowalter[16] used experimental data to calculate and extrapolate a nomograph between methane and water. This nomograph is widely used in the petroleum industry to estimate the interfacial tension of the methane−water system. To validate our model, we selected a number of points in Schowalter's nomograph and calculated the interfacial tension at the corresponding temperatures and pressures using our model (Table 5, Figures 4 and 5). Fluid densities applied in model verification were from the NIST Chemistry WebBook (Table 5). Other parameters are shown in Tables 1−3. According to Table 5, the error of our model ranges from 0 to 10% compared with Schowalter's nomograph.

In order to verify our model under high-pressure conditions, results from the molecular dynamics simulation conducted by Li and Jin[22] were applied to compare with our model at pressure over 65 MPa. Li and Jin carried out molecular dynamics simulation to investigate the interfacial tension of the methane−water system over a wide range of pressures at 298.15 K using a 3.9 nm × 3.9 nm × 31.1 nm simulation cell. For comparison, we used a simulation cell with the same dimension as Li and Jin's study and conducted DPD simulation under their pressure and temperature conditions. Fluid densities utilized in model verification were from the NIST Chemistry WebBook (Table 6). Other parameters are shown in Tables 1−3. Results are shown in Table 6 and Figure 6. Compared with Li and Jin's MD simulation, the error of our model ranges from 0.69 to 10.93%.

Based on the comparisons between our model with Heuer's experimental data,[40] Schowalter's nomograph[16] and Li and Jin's MD simulation,[22] our model is reliable to calculate the interfacial tension of the methane−water system. Moreover, due to the limitations of pressure and temperature in the experiment and nomograph, our model provides access to the methane−water interfacial tension under high-pressure, high-temperature conditions. Although molecular dynamics is also

https://doi.org/10.1021/acsomega.4c03364
ACS Omega 2024, 9, 30794−30803

Table 4. Interfacial Tension Obtained from Experiment and Our Model

pressure (MPa)	temperature (K)	methane density (kg/m^3)	water density (kg/m^3)	interfacial tension obtained through experiment (N/m)	interfacial tension obtained using our model (N/m)	error
0.103	311	0.643	993	0.0675	0.0613	0.0926
5.17	311	34.6	995	0.0569	0.0550	0.0334
10.3	311	73.4	998	0.0512	0.0538	0.0498
13.8	311	100	999	0.0490	0.0513	0.0459

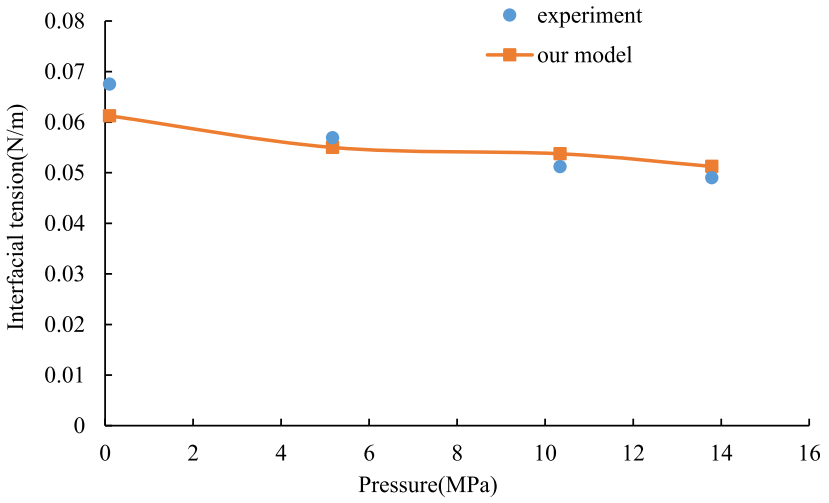

Figure 3. Interfacial tension against pressure obtained from the experiment and our model.

Table 5. Interfacial Tension Obtained from Schowalter's Nomograph and Our Model

pressure (MPa)	temperature (K)	methane density (kg/m^3)	water density (kg/m^3)	interfacial tension obtained using nomograph (N/m)	interfacial tension obtained using our model (N/m)	error
1.41	296	9.42	998	0.070	0.074	0.0536
3.01	305	20.0	996	0.065	0.070	0.0769
5.15	317	33.6	993	0.060	0.060	0
8.19	324	53.4	991	0.055	0.050	0.0909
11.2	333	72.2	988	0.050	0.045	0.1000

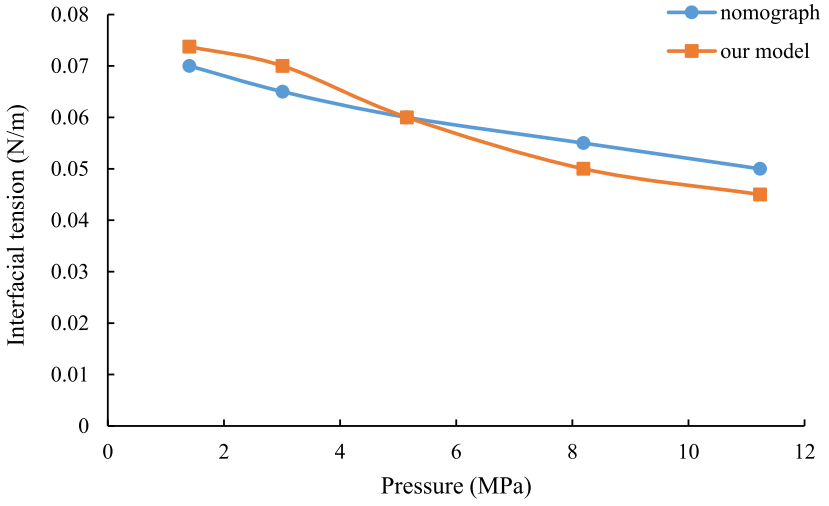

Figure 4. Interfacial tension against pressure obtained from Schowalter's nomograph and our model.

able to calculate the interfacial tension under high-pressure, high-temperature conditions, its computation cost is relatively high. As a result, our model provides reliable and easy access to methane−water interfacial tension for deep shales and other application scenarios.

5. SENSITIVITY STUDY

5.1. Pressure. To investigate the influence of pressure on methane−water interfacial tension during deep shale gas development, we calculated the interfacial tension at pressures 20, 40, 60, 80, 100, and 120 MPa (temperature 423.15 K) using

https://doi.org/10.1021/acsomega.4c03364
ACS Omega 2024, 9, 30794−30803

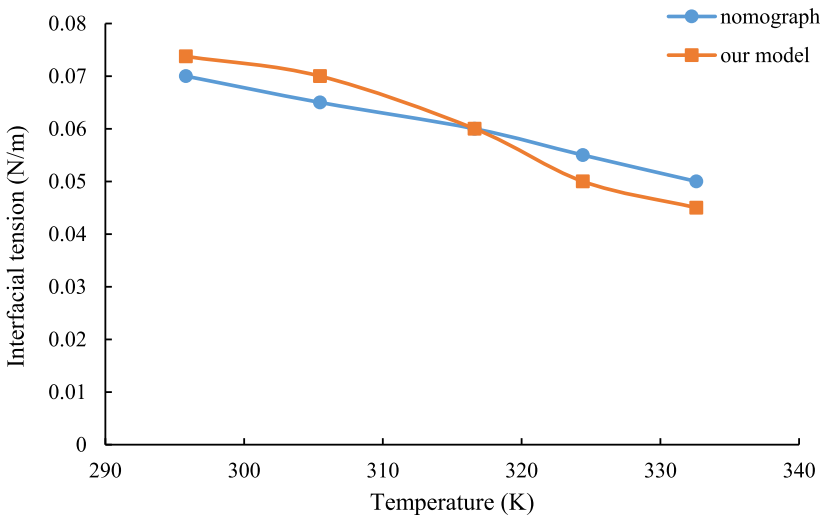

Figure 5. Interfacial tension against temperature obtained from Schowalter's nomograph and our model.

Table 6. Interfacial Tension Obtained from Li and Jin's Molecular Dynamics Simulation and Our Model

pressure (MPa)	temperature (K)	methane density (kg/m^3)	water density (kg/m^3)	interfacial tension obtained through MD simulation (N/m)	interfacial tension obtained using our model (N/m)	error
65.68	298.15	301.63	1024.7	0.0545	0.0605	0.1093
86.58	298.15	328.65	1032.8	0.0537	0.0575	0.0721
161.72	298.15	386.79	1059.5	0.0545	0.0497	0.0875
222.42	298.15	416.22	1078.8	0.0554	0.0546	0.0146
304.03	298.15	445.62	1102.1	0.0562	0.0566	0.0069

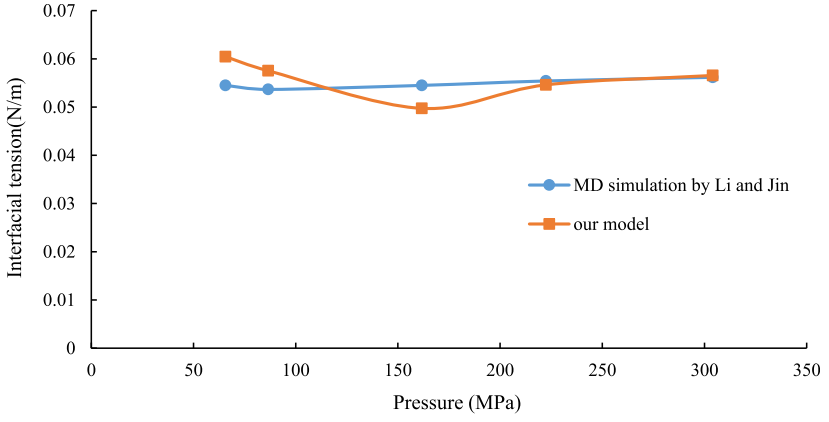

Figure 6. Interfacial tension against pressure obtained from molecular dynamics simulation and our model.

our model (Figure 7). Results indicate that interfacial tension is significantly affected by pressure. It increases from 0.0275 to 0.12 N/m when pressure rises from 20 to 120 MPa. This phenomenon is contrary to the results under conventional conditions (i.e., 0.103−13.8 MPa, 311 K in Figure 3) due to the change of water density. Under conventional conditions in Figure 3, the water density almost remains unchanged from 0.103 to 13.8 MPa. However, under high-temperature, high-pressure conditions, water density increases by 4.9% from 20 to 120 MPa (Figure 8). Water molecules are polar, while methane molecules are nonpolar. The force exerted on the interface molecules by water is much stronger than the force exerted by methane. Therefore, the force exerted by water molecules dominates the interfacial tension of the methane−water system. As a result, the rapid rise in water density contributes to the increase in interfacial tension in Figure 7. This finding is in accordance with the studies conducted by Li and Jin[22] and Kvamme et al.,[24] where they reported an increasing methane−water interfacial tension with a rising pressure under high-pressure conditions.

There exists a turning point (around 40 MPa) as the interfacial tension rises. Interfacial tension increases rapidly when pressure is below 40 MPa, while it increases a little bit slowly if pressure exceeds 40 MPa. This phenomenon could also be explained by the change in fluid densities. The fluid densities and density differences under different pressures are exhibited in Figure 8, in which density data come from the NIST Chemistry WebBook. The density difference between water and methane is smaller at pressures higher than 40 MPa (Figure 8). Therefore, the molecules at the interface are exerted by a lower force. As a result, the rise of interfacial tension at around 40 MPa slows down.

https://doi.org/10.1021/acsomega.4c03364
ACS Omega 2024, 9, 30794−30803

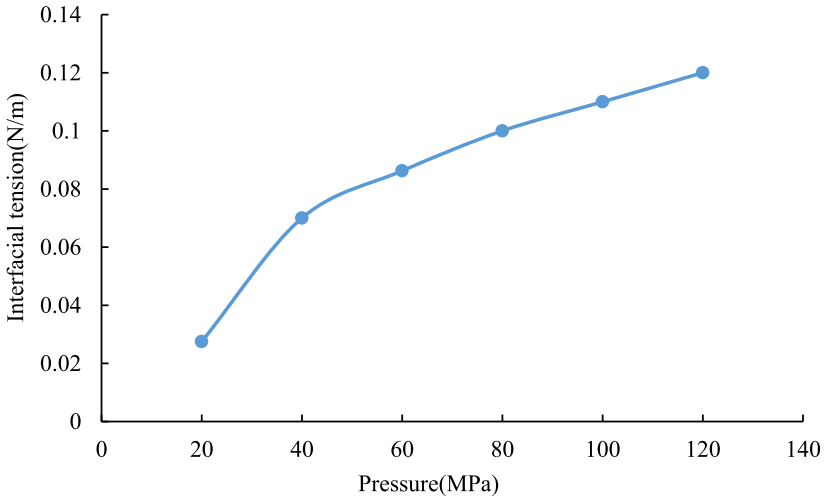

Figure 7. Methane−water interfacial tension against pressure obtained using DPD simulation.

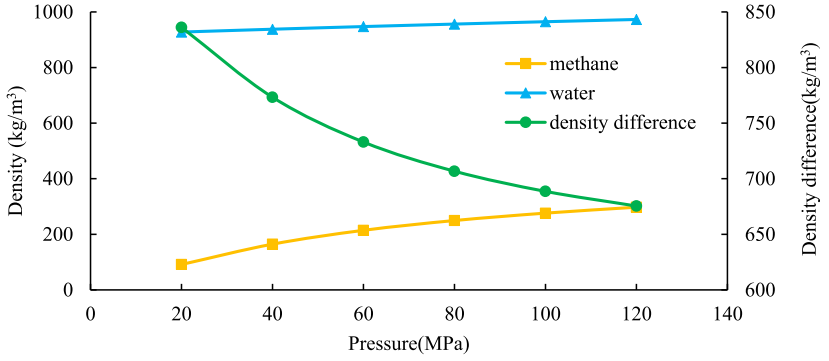

Figure 8. Methane density, water density, and water−methane density difference against pressure.

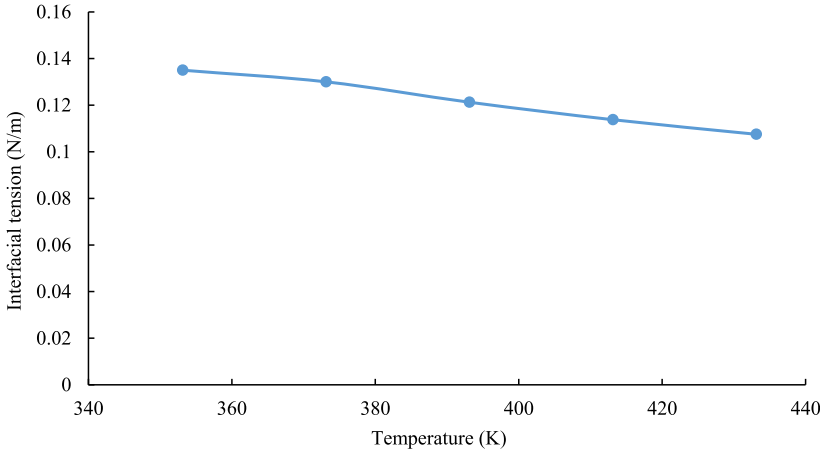

Figure 9. Methane−water interfacial tension against temperature at 100 MPa.

The development of deep shale gas experiences an obvious drop of pressure, and interfacial tension decreases during this period. Because interfacial tensionis closely related to capillary pressure. This indicates that the capillary pressure declines when shale gas production is going on. Hence, the drop in pressure contributes to the gas flow capability and productivity of shale gas wells.

5.2. Temperature. The model was used to study the influence of temperature on interfacial tension. Interfacial tension at temperatures ranging from 353.15 to 433.15 K was computed under a pressure of 100 MPa. Results demonstrate that interfacial tension gradually decreases with the increase of temperature (Figure 9). Because water expands when the temperature rises. This means that the distance between the water molecules becomes larger. Hence, water molecules exert smaller forces on interface molecules, and interfacial tension reduces. This physical phenomenon is also consistent with the previous findings by He[16] and Heuer.[40] Only 20% of interfacial tension is reduced with the temperature increasing from 353.15 to 433.15 K. Because the variation of temperature is very slight during the development of deep shale gas, the interfacial tension can be regarded as a constant value.

https://doi.org/10.1021/acsomega.4c03364
ACS Omega 2024, 9, 30794−30803

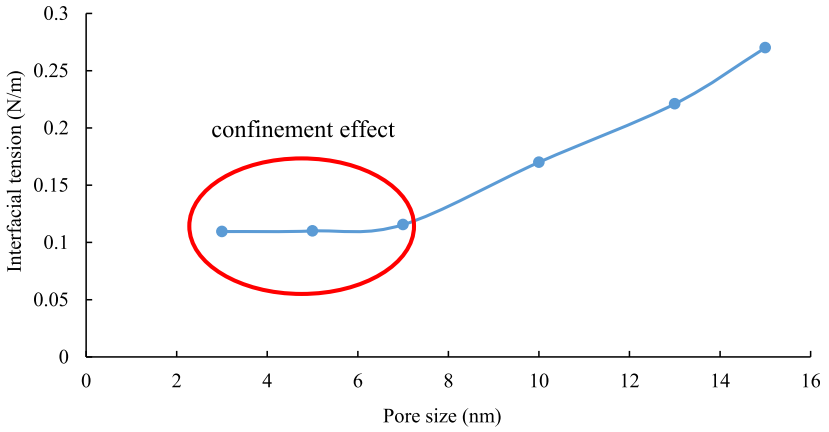

Figure 10. Methane−water interfacial tension against pore size ranging from 3 to 15 nm.

5.3. Pore Size. Interfacial tension affected by pore size was investigated using DPD simulation. Simulation cells with sizes of 3, 5, 7, 10, 13, and 15 nm were built to approximate the real pore size in deep shales.[38] Results are shown in Figure 10, where the confinement effect is observed. The confinement effect refers to the phenomenon that when the size of space is on the order of only one or several nanometers, the phase behavior of matter as well as the energy landscape of either a chemical reaction or a physical process may be different from their analogues in bulk.[41] Due to the confinement effect, interfacial tension almost remains unchanged at pore sizes ranging from 3 to 7 nm. Interfacial tension rises when pore size increases from 7 to 15 nm. Because the interfacial tension can be regarded as the sum of forces exerted on the interfacial layer molecules by the molecules out of the interface layer. If the pore size is between 3 and 7 nm, fluids are confined to a very small space. The interface layer molecules occupy most of the pore volume. The quantity of molecules outside the interface layer is very limited. As a result, the interfacial tension remains almost unchanged. When pore size becomes larger, i.e., above 7 nm, there are more molecules out of the interface layer. The forces exerted on interface layer molecules become higher. Therefore, the interfacial tension rises when the pore size is larger than 7 nm, and the confinement effect is reduced. When the pore size increases from 7 to 15 nm, the interfacial tension experiences a growth from 0.1155 to 0.27 mN/m. Interfacial tension is a key parameter to affect capillary pressure. This phenomenon also indicates that the capillary pressure increases when gas flows in pores ranging from 7 to 15 nm.

6. CONCLUSIONS

1. The DPD model established in this article can be used to predict the methane−water interfacial tension in nanopores with high accuracy and low computation cost.
2. Pressure has a significant influence on methane−water interfacial tension. Interfacial tension increases from 0.0275 to 0.12 N/m when pressure rises from 20 to 120 MPa. This suggests that during the development of deep shale gas, the pressure drop helps to improve the flow capability of shale gas.
3. The interfacial tension slightly decreases with an increase of temperature. Because the change in temperature is not obvious in deep shale gas development, its impact on interfacial tension can be negligible.
4. The interfacial tension is affected by pore size. It remains unchanged when pore size is smaller than 7 nm owing to the confinement effect, while it increases if pore size exceeds 7 nm. This indicates that fluid flow in the pores with a size between 7 and 15 nm encounters an increasing capillary pressure, which reduces gas flow capability.

AUTHOR INFORMATION

Corresponding Author

Fei Mo − *School of Petroleum Engineering, Chongqing University of Science and Technology, Chongqing 401331, P. R. China*; orcid.org/0000-0003-4779-5106; Email: mofei_cqust@163.com

Authors

Zhilin Qi − *School of Petroleum Engineering, Chongqing University of Science and Technology, Chongqing 401331, P. R. China*

Xiaoliang Huang − *School of Petroleum Engineering, Chongqing University of Science and Technology, Chongqing 401331, P. R. China*

Wende Yan − *School of Petroleum Engineering, Chongqing University of Science and Technology, Chongqing 401331, P. R. China*

Wanliang Zhang − *School of Petroleum Engineering, Chongqing University of Science and Technology, Chongqing 401331, P. R. China*

Chaowen Wang − *Petroleum Engineering School, Southwest Petroleum University, Chengdu 610500, P. R. China*

Wenting Fu − *School of Petroleum Engineering, Chongqing University of Science and Technology, Chongqing 401331, P. R. China*

Complete contact information is available at: https://pubs.acs.org/10.1021/acsomega.4c03364

Notes

The authors declare no competing financial interest.

ACKNOWLEDGMENTS

This work was financially supported by the National Natural Science Foundation of China (grant nos. 52204035 and 52274034).

https://doi.org/10.1021/acsomega.4c03364
ACS Omega 2024, 9, 30794−30803

REFERENCES

(1) Mu, Z.; Ning, Z.; Lyu, F.; Liu, B. Sorption of deep shale gas on minerals and organic matter from molecular simulation. *Energy Fuels* **2023**, *37*, 251−259.

(2) Zhan, G.; Yang, J.; Zhao, Y.; Zhang, N.; Wang, B.; Li, S. Development practice and challenges of deep shale gas in southern Sichuan Basin. *Pet. Geol. Exp.* **2023**, *45* (6), 1067−1077.

(3) Al-Ameri, A.; Gamadi, T.; Ispas, I.; Watson, M. A workflow to investigate the impact of the spontaneous imbibition of a slickwater fracturing fluid on the near fracture face shale matrix. In *SPE Eastern Regional Meeting*: Pittsburgh, Pennsylvania, USA, 2018.

(4) Gupta, A.; Xu, M.; Dehghanpour, H.; Bearinger, D. Experimental investigation for microscale stimulation of shales by water imbibition during the shut-in periods. *SPE Unconventional Resources Conference*: Calgary, Alberta, Canada, 2017.

(5) Li, X.; Abass, H.; Teklu, T. W.; Cui, Q. A shale matrix imbibition model-interplay between capillary pressure and osmotic pressure. *SPE Annual Technical Conference & Exhibition*: UAE, Dubai, 2016.

(6) Roychaudhuri, B.; Tsotsis, T. T.; Jessen, K. An experimental investigation of spontaneous imbibition in gas shales. *J. Pet. Sci. Eng.* **2013**, *111*, 87−97.

(7) Dehghanpour, H.; Lan, Q.; Saeed, Y.; Fei, H.; Qi, Z. Spontaneous imbibition of brine and oil in gas shales: effect of water adsorption and resulting microfractures. *Energy Fuels* **2013**, *27* (6), 3039−3049.

(8) Mo, F.; Qi, Z.; Huang, X.; Yan, W.; Wang, S.; Yuan, Y.; Li, Z. Knudsen diffusion in pore-scale water-bearing shales: modelling and case study. *J. Pet. Sci. Eng.* **2022**, *214*, 110457−110458.

(9) Mo, F.; Qi, Z.; Yan, W.; Huang, X.; Li, J. Influence of Water on Gas Transport in Shale Nanopores: Pore-Scale Simulation Study. *Energy Fuels* **2020**, *34*, 8239−8249.

(10) Isfehani, Z. D.; Sheidaie, A.; Hosseini, M.; Fahimpour, J.; Iglauer, S.; Keshavarz, A. Interfacial tensions of (brine+h2+co2) systems at gas geo-storage conditions. *J. Mol. Liq.* **2023**, *374*, 121279.

(11) Pan, Z.; Trusler, J. M. Experimental and modelling study of the interfacial tension of (n-decane + carbon dioxide + water) in the three phase region. *Fluid Phase Equilib.* **2023**, *568*, 113760−113812.

(12) Sauerer, B.; Mohammed, A.; Mark, M. S.; Wael, A. Effect of formation water salinity on interfacial tension of reservoir fluids. *J. Pet. Sci. Eng.* **2021**, *204*, 108700.

(13) Liu, Y. Research on surface tension measurement method and application of liquid droplet based on ultrasonic radiation force. Master's dissertation, University of Chinese Academy of Sciences, 2022.

(14) Has, C. Microfluidic approaches for measuring the interfacial tension in-fluid-fluid systems: a concise review. *Fluid Mech. Res.* **2021**, *48* (2), 83−100.

(15) Chow, Y. F.; Maitland, G. C.; Trusler, J. M. Interfacial tensions of (H2O+H2) and (H2O+ CO2+H2) systems at temperatures of (298−448) K and pressures up to 45 MPa. *Fluid Phase Equilib.* **2018**, *475*, 37−44.

(16) He, G.; Tang, H. *Petrophysics*; Petroleum Industry Press: Beijing, 2019.

(17) Dong, J.; Liu, X.; Zhao, T.; Wen, B.; Han, H. Optimization of Experimental Conditions for Determination of Surface Tension of Solution by the Maximum Bubble Pressure Method. *Univ. Chem.* **2021**, *36* (6), 2007002.

(18) Marquez, R.; Forgiarini, A. M.; Langevin, D.; Salager, J. L. Breaking of water-in-crude oil emulsions. part 9. new interfacial rheology characteristics measured using a spinning drop rheometer at optimum formulation. *Energy Fuels* **2019**, *33* (9), 8151−8164.

(19) Dreher, T.; Lemarchand, C.; Pineau, N.; Bourasseau, E.; Ghoufi, A.; Malfreyt, P. Calculation of the interfacial tension of the graphene-water interaction by molecular simulations. *J. Chem. Phys.* **2019**, *150* (1), 14703.

(20) Ghoufi, A.; Malfreyt, P. Interfacial tension of the graphene-water solid-liquid interface: how to handle the electrostatic interactions? *Mol. Phys.* **2021**, *119* (19−20), 1−12.

(21) Chiricotto, M.; Giunta, G.; Karimi-Varzaneh, H. A.; Carbone, P. Calculation of the work of adhesion of polyisoprene on graphite by molecular dynamics simulations. *Soft Mater.* **2020**, *18* (2−3), 140−149.

(22) Li, W.; Jin, Z. Molecular dynamics simulations of natural gas-water interfacial tensions over wide range of pressures. *Fuel* **2019**, *236*, 480−492.

(23) Doan, Q. T.; Keshavarz, A.; Miranda, C. R.; Behrenbruch, P.; Iglauer, S. Molecular dynamics simulation of interfacial tension of the CO2-CH4-water and H2-CH4-water systems at the temperature of 300 K and 323 K and pressure up to 70 MPa. *J. Energy Storage* **2023**, *66*, 107470.

(24) Kvamme, B.; Kuznetsova, T.; Schmidt, K. Molecular Dynamics Simulations and Numerical Modelling of Interfacial Tension in Water-Methane Systems. *4th WSEAS Transactions on Biology and Biomedicine*, 2007; Vol. 3(7), pp 517−523.

(25) Guo, Q.; Hu, W.; Zhang, Y.; Zhang, K.; Dong, B.; Qin, Y.; Li, W. Molecular dynamics simulation of the interfacial properties of methane-water and methane-brine systems. *Mol. Simul.* **2023**, *49* (12), 1215−1228.

(26) Naeiji, P.; Woo, T. K.; Alavi, S.; Varaminian, F.; Ohmura, R. Interfacial properties of hydrocarbon/water systems predicted by molecular dynamic simulations. *J. Chem. Phys.* **2019**, *150* (11), 114703.

(27) Liu, M.; Chang, J.; Liu, H. DPD simulation of multiphase flow at small scales. *2nd International Conference on Computer and Automation Engineering (ICCAE)*, 2010; Vol. 5, pp 334−337.

(28) Deguillard, E.; Pannacci, N.; Creton, B.; Rousseau, B. Interfacial tension in oil-water-surfactant systems: on the role of intra-molecular forces on interfacial tension values using DPD simulations. *J. Chem. Phys.* **2013**, *138* (14), 2155−2168.

(29) Rezaei, H.; Modarress, H. Dissipative particle dynamics (dpd) study of hydrocarbon-water interfacial tension (ift). *Chem. Phys. Lett.* **2015**, *620*, 114−122.

(30) Wang, S.; Yang, S.; Wang, X.; Liu, Y.; Yang, S.; Dong, Q. Numerical simulations of the effect of ionic surfactant/polymer on oil-water interface using dissipative particle dynamics. *Asia-Pac. J. Chem. Eng.* **2016**, *11* (4), 581−593.

(31) Dzwinel, W.; Yuen, D. A. A two-level, discrete-particle approach for simulating ordered colloidal structures. *J. Colloid Interface Sci.* **2000**, *225* (1), 179−190.

(32) Groot, R.; Warren, P. Dissipative particle dynamics: Bridging the gap between atomistic and mesoscopic simulation. *J. Chem. Phys.* **1997**, *107* (11), 4423−4435.

(33) Español, P.; Warren, P. Statistical mechanics of dissipative particle dynamics. *Europhys. Lett.* **1995**, *30* (4), 191−196.

(34) Groot, R.; Madden, T. Dynamic Simulation of Diblock Copolymer Microphase Separation. *J. Chem. Phys.* **1998**, *108* (20), 8713−8724.

(35) Maiti, A.; McGrother, S. Bead-bead Interaction Parameters in Dissipative Particle Dynamics: Relation to Bead-size, Solubility Parameter, and Surface Tension. *J. Chem. Phys.* **2004**, *120* (3), 1594−1601.

(36) Iglauer, S.; Mathew, M.; Bresme, F. Molecular dynamics computations of brine-co2 interfacial tensions and brine-co2-quartz contact angles and their effects on structural and residual trapping mechanisms in carbon geo-sequestration. *J. Colloid Interface Sci.* **2012**, *386* (1), 405−414.

(37) See http://www.accelrys.com for more information.

(38) Shi, X.; Wu, W.; Hu, H.; Liu, L.; Zhu, Y.; Pan, R.; Meng, J.; Wang, T. The whole Apertures of Deeply Buried Wufeng-Longmaxi Formation Shale and Their Controlling Factors in Luzhou District, Sichuan Basin. *Earth Sci.* **2023**, *48* (1), 158−172.

(39) Wang, X. Study on the effect of non-uniform conductivity of deep shale gas fracture on productivity. Master's dissertation, China University of Petroleum, 2019.

(40) Heuer, G. J. Interfacial tension of water against hydrocarbon and other gases and adsorption of methane on solids at reservoir temperatures and pressures. Doctor's dissertation, The University of Texas, 1957.

https://doi.org/10.1021/acsomega.4c03364
ACS Omega 2024, 9, 30794−30803

(41) Qian, J.; Gao, X.; Pan, B. Nanoconfinement-Mediated Water Treatment: From Fundamental to Application. *Environ. Sci. Technol.* **2020**, *54* (14), 8509−8526.

https://doi.org/10.1021/acsomega.4c03364
ACS Omega 2024, 9, 30794−30803